

the oxidation peak of BPA showing the good reproducibility in preparing the ERGO-SbNPs-PGE. The modified electrodes were stored in a refrigerator in between the measurements.

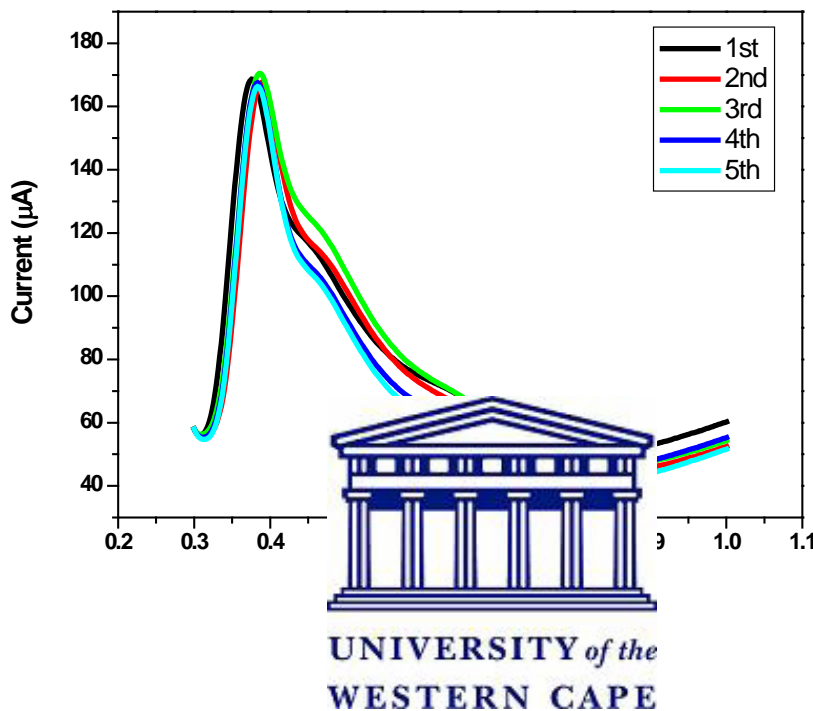


Figure 6.19: DPV of 0.1 molL^{-1} PBS at pH 7 containing $50 \text{ }\mu\text{M}$ BPA at single- use ERGO-SbNPs-PGE.

6.3.12. Preconcentration time optimization

The influence of pre-concentration time on the peak current of BPA while stirring was investigated over the time interval from 30 to 180 seconds (Figure 6.20). A significant enhancement of adsorptive stripping peaks was observed as the pre-concentration time increased since, a longer time allowed for more BPA to be adsorbed onto the electrode surface. As the peak heights has not increased significantly after 60 seconds a pre-concentration time of 60 s was chosen for further analysis.

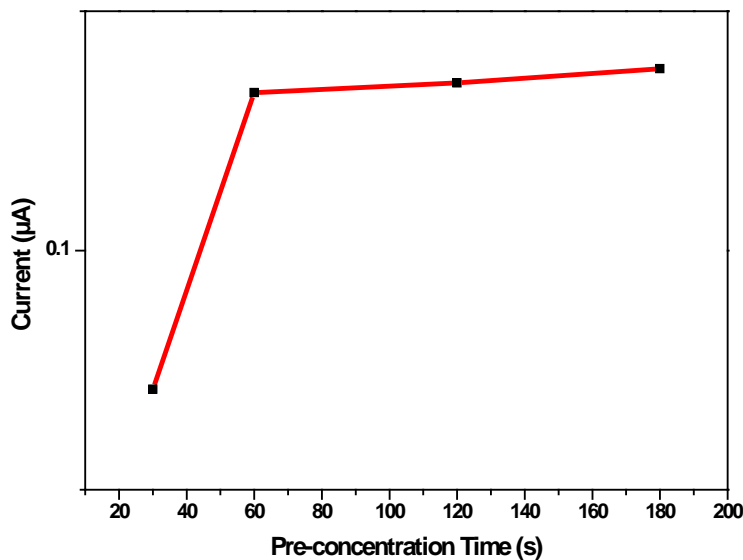


Figure 6.20: Effect of pre-concentration time on the peak current of 5.0 μM BPA in 10 mL 0.1 M PBS at ERGO-SbNPs-PGE using DPV.

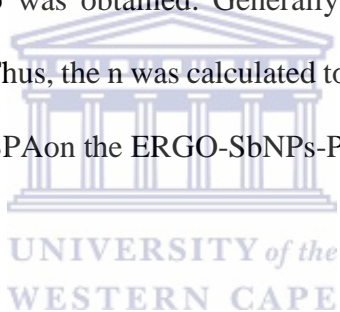
6.3.13. Effect of scan rate on the electrocatalytic oxidation of BPA at ERGO-SbNPs-PGE

Figure 6.21 shows the cyclic voltammograms of BPA at the ERGO-SbNPs-PGE when the scan rate (ν) varies from 10 to 100 mVs^{-1} . As is shown in Fig 6.21 (a), the oxidation peak currents increased linearly in an irreversibly electrode process, indicating that the oxidation of BPA at the ERGO-SbNPs-PGE is adsorption-controlled. Moreover, not linearity of the plot of the peak current (I_{pa}) against the square root of scan rate ($\nu^{1/2}$), confirms the adsorption-controlled BPA oxidation (Fig 6.21 (d)) [52,114,115]. The linear regression equations for oxidation peak (I_{pa}) current is: $I_{\text{pa}} = 409.44 \nu + 1.6547$ with the correlation coefficients of 0.9984 (Fig 6.21 (b)). As shown in figure 6.21 (c) there is a linear relationship between the peak potential (E_{p}) and the natural logarithm of

scan rate ($\ln v$) for the ERGO-SbNPs-PGE. As for an irreversibly electrode process, the number of electrons involved in the reaction can be estimated according to the Laviron's equation as follows:

$$E_p = E^0 + (RT/\alpha nF) [\ln (RTk_s/\alpha nF) - \ln v] \quad (\text{Eqn. 6.1})$$

Where α is the electron transfer coefficient, k_s is the standard rate constant of the surface reaction, T is the temperature (298 K here), v is the scan rate, R the gas constant ($8.314 \text{ JK}^{-1}\text{mol}^{-1}$), n is the electron transfer numbers, F the Faraday constant ($96,480 \text{ C mol}^{-1}$) and E^0 the formal redox potential. The αn value can be calculated from the slope of the linear regression equation of the linear plot of E_p with respect to $\ln v$ of $E_p = 0.0248 \ln(v) + 0.4649$, $R^2 = 0.998$. $RT/\alpha nF$ was 0.0248 here, then the value of $\alpha n = 1.035$ was obtained. Generally, for a totally irreversible electron transfer, α was assumed to be 0.5. Thus, the n was calculated to be 2.07 showing that two electrons were involved in the oxidation of BPA on the ERGO-SbNPs-PGE.



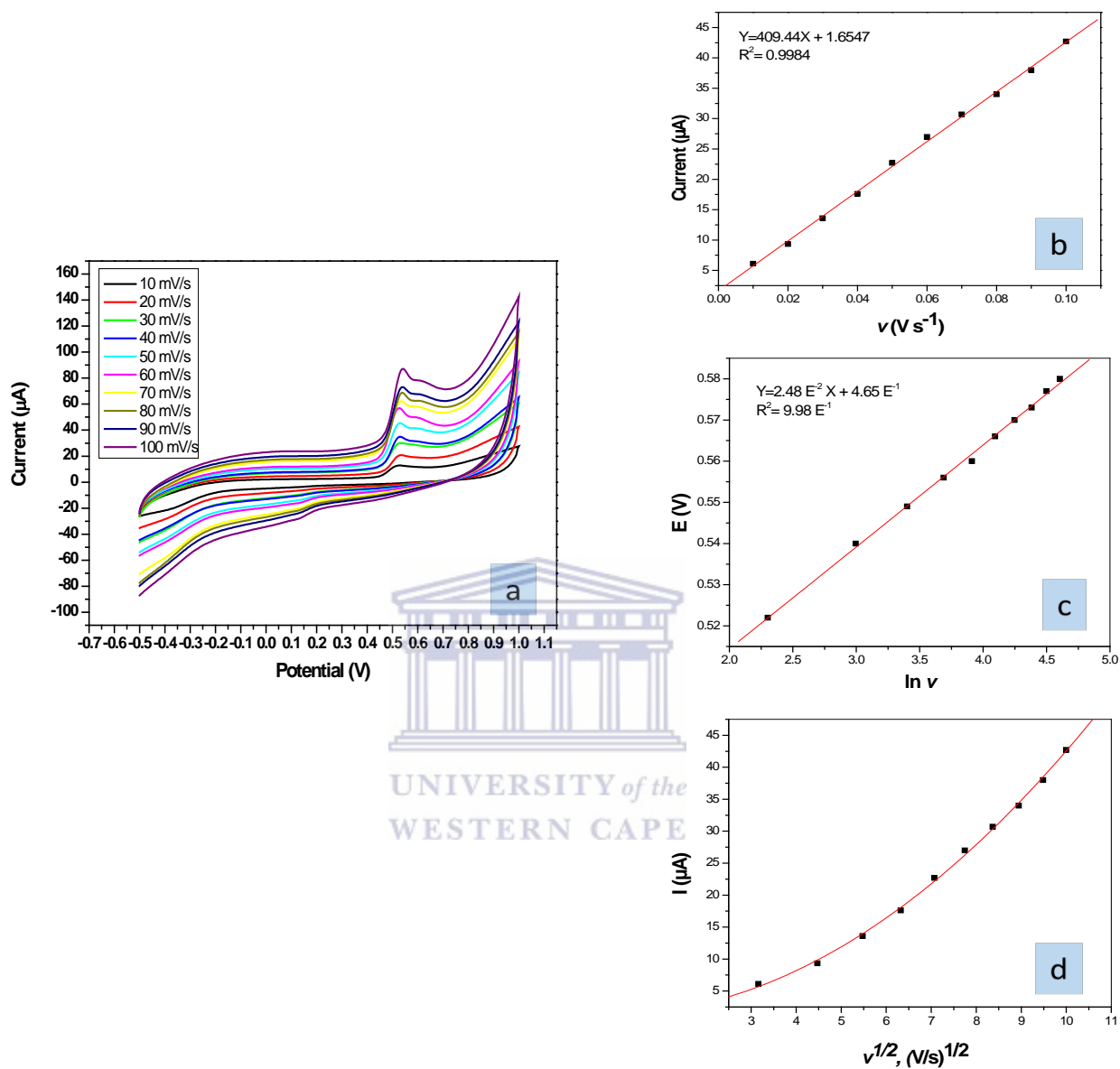


Figure 6.21: (a) Cyclic voltammetric responses of 10 μM BPA at ERGO-SbNPs-PGE in 0.1 M PBS (pH= 7.0) at scan rates, (inner to outer) 10, 20, 30, 40, 50, 60, 70, 80, 90, 100 mVs^{-1} . (b and d) The plots of peak currents vs scan rate and square root of scan rate, respectively. (c) The variation of peak potential vs $\ln v$.

6.3.14. pH optimization

The effect of pH on the adsorptive stripping peak current (I_p) and peak potential was studied by differential pulse voltammetry measurements at pH ranging from 5 to 10 containing 5.0 μM BPA (Figure 6.22). The highest peak current (I_p) was observed at 7.04. Therefore pH 7.04 was chosen as the optimum pH for use in subsequent BPA measurements. The linear shifting of the peak potential to more negative values with increasing pH with a slope of -61.24 mV/pH which was close to the theoretical value 57 mV/pH indicates equal number of protons and electrons are involved in the BPA oxidation (a two-electron-two-proton process) [11,86,115].

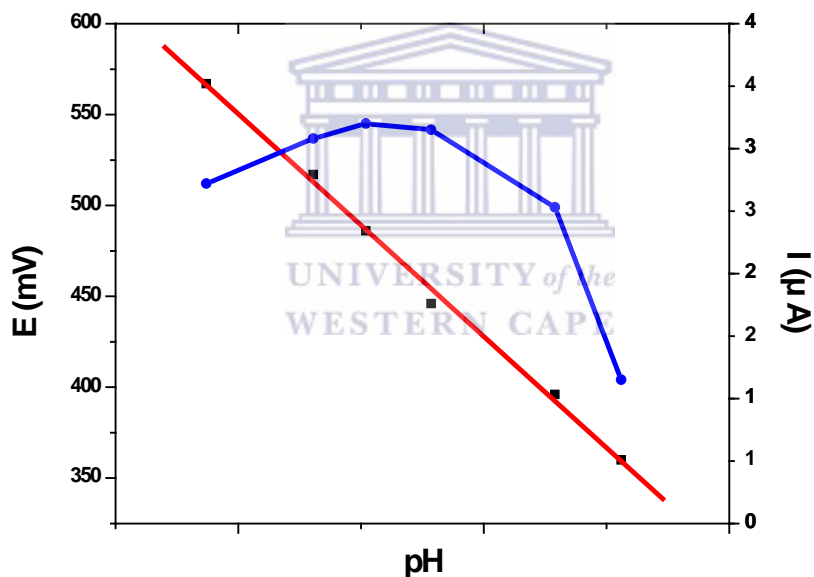


Figure 6.22: Effect of pH on the peak current (blue) and peak potential (red) of 1.0 μM BPA in 10 mL 0.1 M PBS at ERGO-SbNPs-PGE using DPV.

6.3.15. Interference studies

The effect of various possible interfering molecules was examined on the determination of 50 μM bisphenol A by DPV measurements in the absence and presence of the interferences (Figure 6.23). The electroinactive molecules that were tested were as following: O-Nitrophenol, Potassium Chloride, Cerium (III) nitrate hexahydrate, sodium chloride, 4-cumylphenol. As it shown in the Figure 8 no electroactivity and change was found in the voltammetric response of 50 μM BPA in the presence of two-time excess concentration (100.0 μM) of these species except 4-cumylphenol. The oxidation peak response of the BPA increased significantly in the presence of 4-cumylphenol indicating the interfering effect of 4-cumylphenol on electrode response towards BPA measurement.



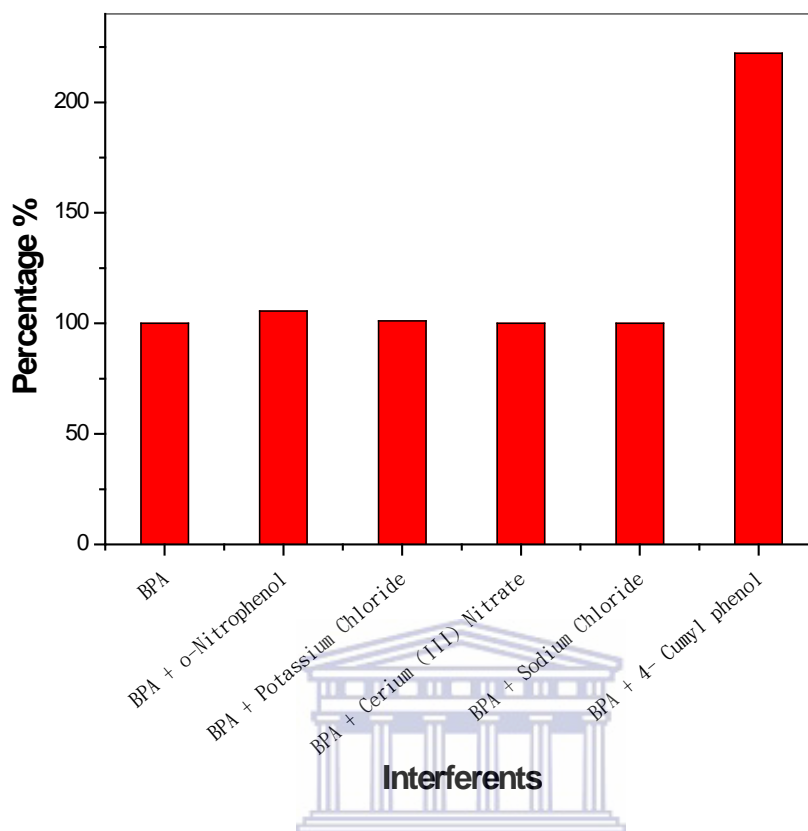


Figure 6.23: Percentages of the oxidation peak current of 50 μM of the BPA in absence and presence of 100 μM O-Nitrophenol, Potassium Chloride, Cerium (III) nitrate hexahydrate, sodium chloride, 4-cumylphenol.

6.3.16. Detection limit

The detection limit was calculated from BPA calibration curve using the DPV optimized conditions as previously described at the rGO-SbNPs-PGE electrode to investigate its electrochemical response as a function of the BPA concentration (0.4 μM to 5.0 μM). As it was shown in Figure 6.24 there was a linear relationship between the BPA concentration and peak current with a correlation coefficient of 0.999 ($n = 9$).

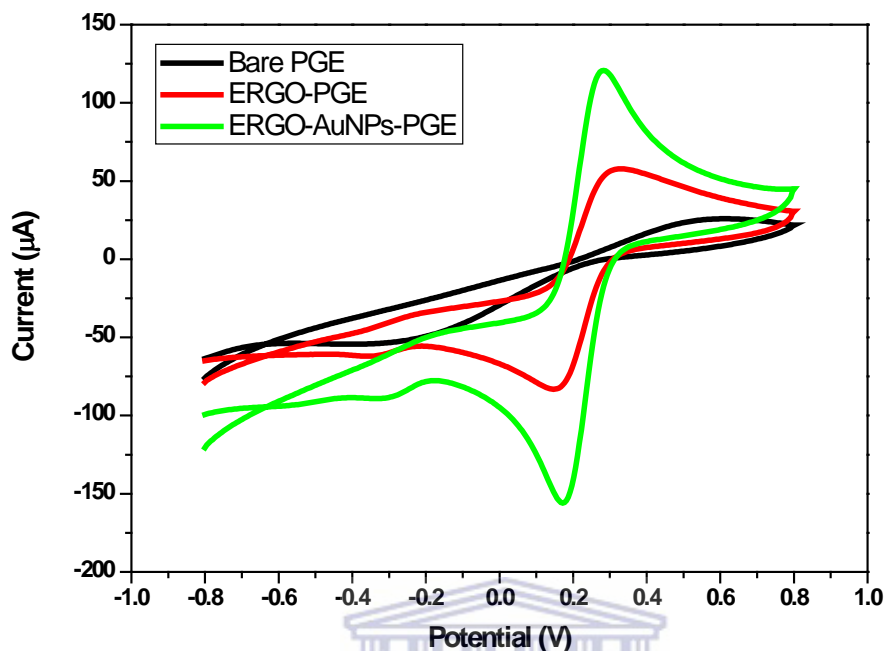


Figure 6.26: Cyclic voltammetry at bare PGE (black), ERGO-PGE in absence of AuNPs (red) and ERGO-AuNPs-PGE (green) in 5.0 mM $\text{Fe}(\text{CN})_6$ in 0.1 M KCl solution.

6.4.2. Impedimetric analysis

Figure 6.27 shows electrochemical impedance analysis of the bare PGE, ERGO-PGE, and ERGO-AuNPs-PGE in 0.1 M KCl solution containing 5 mM $[\text{Fe}(\text{CN})_6]^{3-/4-}$. The electrochemical properties of the film modified on the pencil graphite electrode are studied by using the associated equivalent circuit model. The semicircle parameters of the Nyquist plots of the bare PGE, ERGO-PGE, and ERGO-AuNPs-PGE correspond to the double layer capacity (C_{dl}) of the film and the electron transfer resistance (R_{ct}) [109–111]. A semicircle area ($R_{ct} = 1971.9 \Omega$) is observed at bare PGE which is larger than ERGO film ($R_{ct} = 458.94 \Omega$); this area has decreased at ERGO-AuNPs

film ($R_{ct} = 224.04 \Omega$) in comparison to other two electrodes indicating the lower electron transfer resistance at ERGO-AuNPs film which improves the electron- transfer kinetics process as a faster one and more suitable for the electrocatalytic activities, respectively [110,112,113].

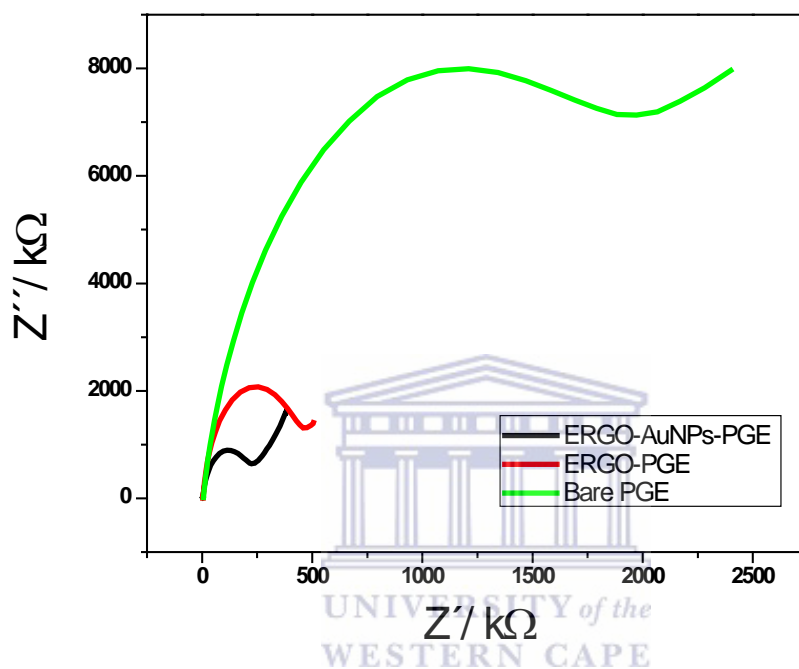


Figure 6.27: EIS response of the bare PGE (green), and ERGO-PGE (red), and ERGO-AuNPs-PGE (black) in 0.1 M KCl containing 5 mM $[\text{Fe}(\text{CN})_6]^{3-/4-}$.

6.4.3. The effect of scan rate

It is shown in Figure 6.28a the CV measurements of the 5 mM $\text{K}_3\text{Fe}(\text{CN})_6$ at ERGO-AuNPs-PGE at different scan rates from 10 to 100 mV s^{-1} . The linear relationship between the square root of the scan rate and oxidation and reduction peak current of $\text{K}_3\text{Fe}(\text{CN})_6$ (Fig. 6.28b) indicates that the process is diffusion controlled[15]. Anodic and cathodic peak current versus the square root of the scan rate obtained a correlation of 0.9998 and 0.998, respectively.

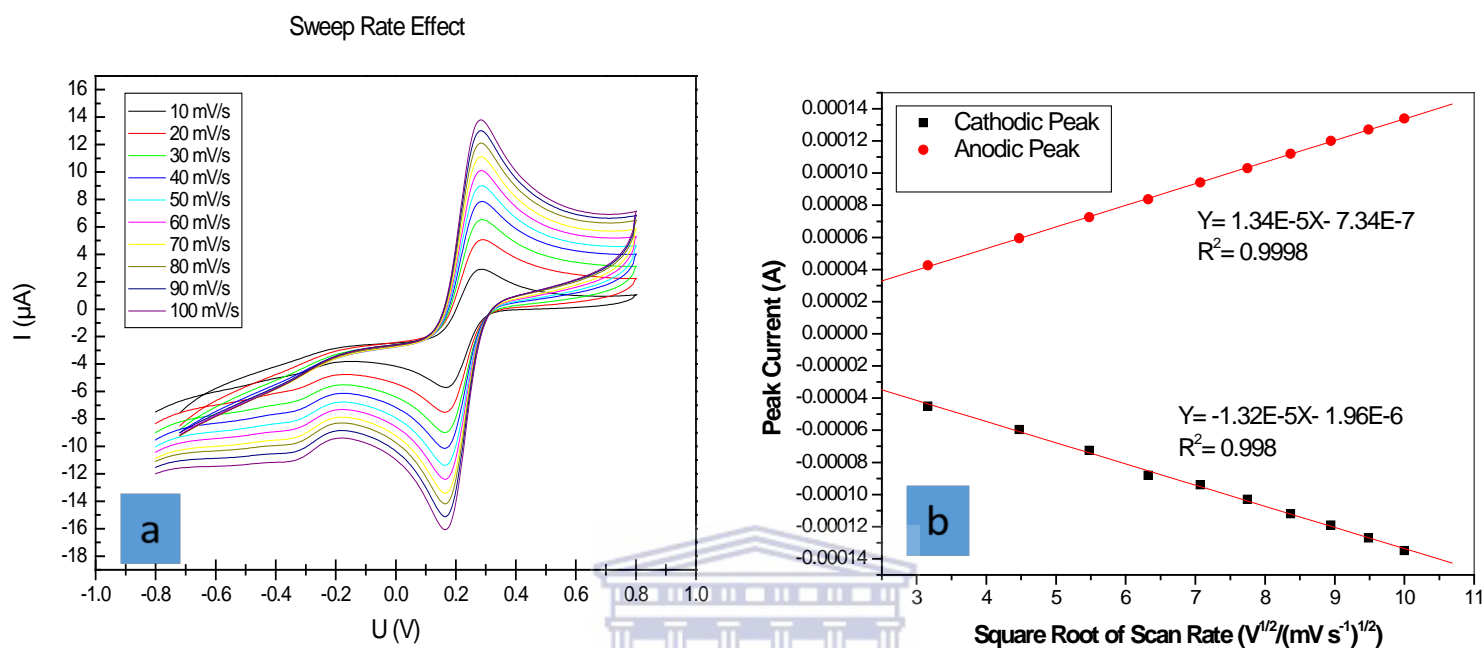


Figure 6.28: Cyclic voltammograms overlay at different scan rates from 10 to 100 mV s⁻¹ in 10 mL 0.1 M KCl solution containing 5.0 mM [Fe (CN) ₆]^{3-/4-} at ERGO-AuNPs-PGE (a) and The plot of peak currents vs square root of scan rate (b).

6.4.4. Influence of the number of GO-AuNPs electrodeposition cycles

The effect of the number of cycles to modify the pencil graphite electrode with GO-AuNPs on the oxidation peak of BPA was investigated in a 0.1 M phosphate buffer solution (pH 7) containing 50 μg L⁻¹ BPA (Figure 6.29). The optimum number of cycles of 5 was selected for the further analysis as the peak heights decreased after 5 cycles due to the ERGO-AuNPs film thickness causing less electron flow to the electrode surface.

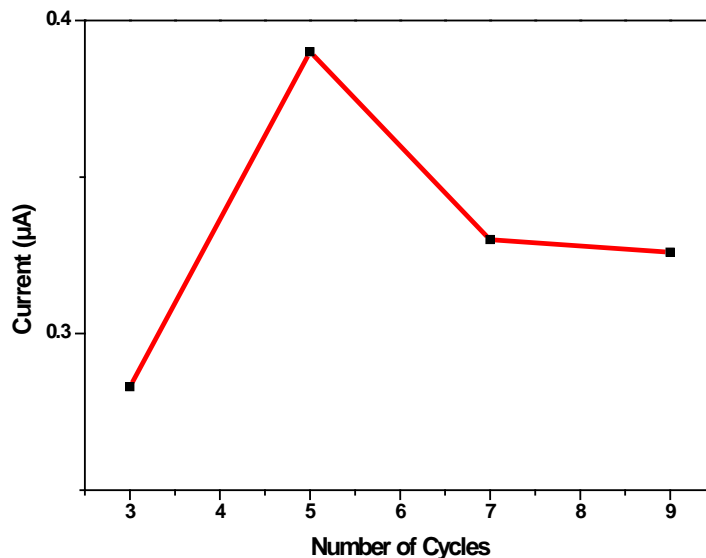
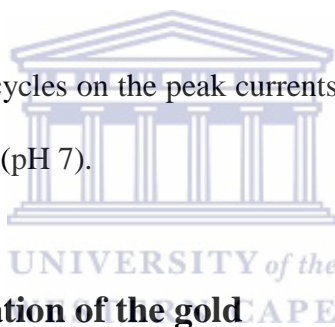


Figure 6.29: Effect of number of cycles on the peak currents of BPA at the ERGO-AuNPs-PGE in 0.1 M phosphate buffer solution (pH 7).



6.4.5. Effect of the concentration of the gold

The influence of gold concentration in the GO-AuNPs solution before its electrodeposition onto the pencil graphite electrode was studied in a 0.1 M phosphate buffer solution (pH 7) containing $50 \mu\text{g L}^{-1}$ BPA (Figure 6.30). It was observed in Figure 10 that the electrochemical response of BPA at ERGO-AuNPs-PGE changes with increasing the gold concentration in GO-AuNPs solution. A 15 ppm concentration of Au solution gives the highest oxidation peak current. The gold nanoparticles sizes probably enlarge with increasing the gold concentration in the solution and it causes the shorter oxidation peak heights at solution concentrations greater than 15 ppm of Au [80,81,108].

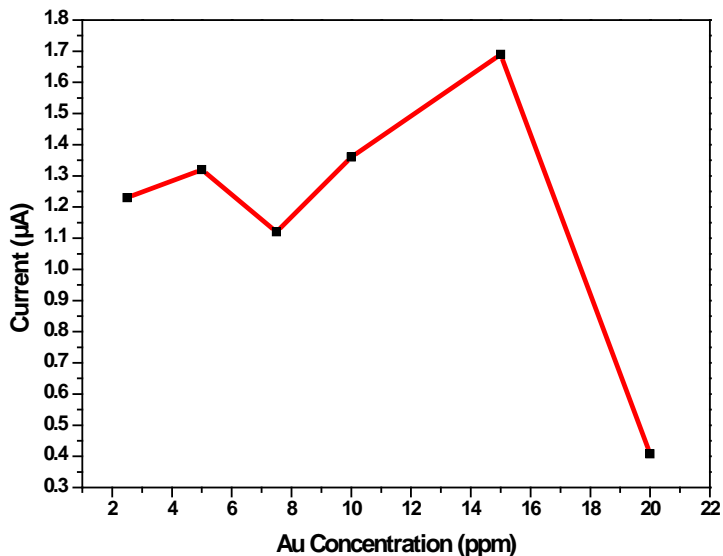
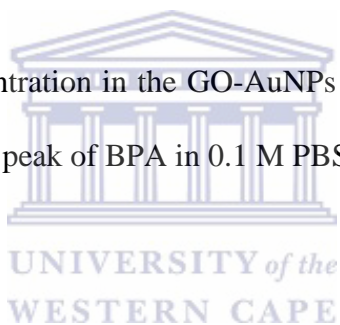


Figure 6.30: Effect of gold concentration in the GO-AuNPs solution for modification of pencil graphite electrode on the oxidation peak of BPA in 0.1 M PBS (pH 7) containing $50 \mu\text{g L}^{-1}$ BPA.



6.4.6. The effect of the electrodeposition time of GO-AuNPs

The effect of the electrodeposition time of GO-AuNPs varying from 30 s to 300 s for the modification of the pencil graphite electrode on the oxidation peak of BPA was investigated in a 0.1 M phosphate buffer solution (pH 7) containing $50 \mu\text{g L}^{-1}$ BPA (Figure 6.31). The peak currents increased to a maximum at 120 s with increasing the electrodeposition time followed by the decrease in peak current with increasing the electrodeposition time more than 120 s suggesting surface saturation of the electrode. The optimal deposition time of 120 s was chosen for further analysis.

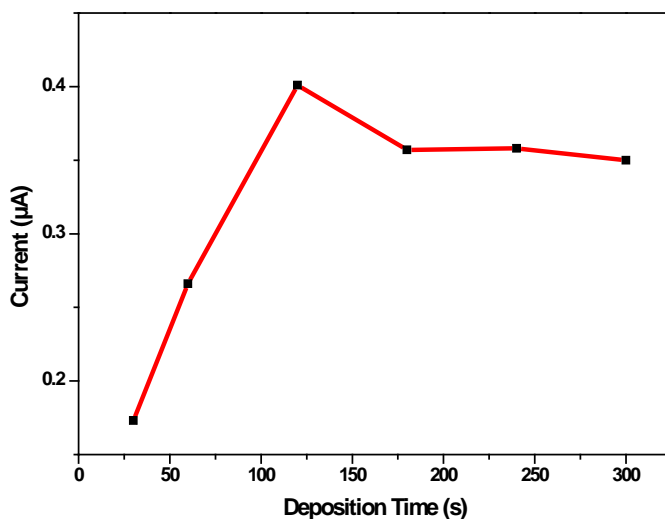


Figure 6.31: Effect of the electrodeposition time of GO-AuNPs for modification of pencil graphite electrode on the oxidation peak of BPA in 0.1 M PBS (pH 7) containing $50 \mu\text{g L}^{-1}$ BPA.



6.4.7. Microscopic Characterization of Electrodeposited Graphene- AuNPs Modified Pencil Electrode (ERGO-AuNPs-PGE)

The high resolution scanning electron microscopy (HRSEM) images of the bare PGE, ERGO-PGE and ERGO-AuNPs-PGE surfaces are shown in Figure 6.32. Surface roughness with grooves on the surface along the direction of machining can be observed at the bare PGE surface (Figure 6.32a). Following the electrochemical reduction of graphene oxide, flakes of graphene sheets can be seen at the ERGO-PGE surface at high magnification (Fig 6.32b). Gold nanoparticles on top of the graphene sheets are observed at the ERGO-AuNPs-PGE (Figure 6.32c). The gold nanoparticles sizes varies from 20 to 50 nm (Fig 6.32d)

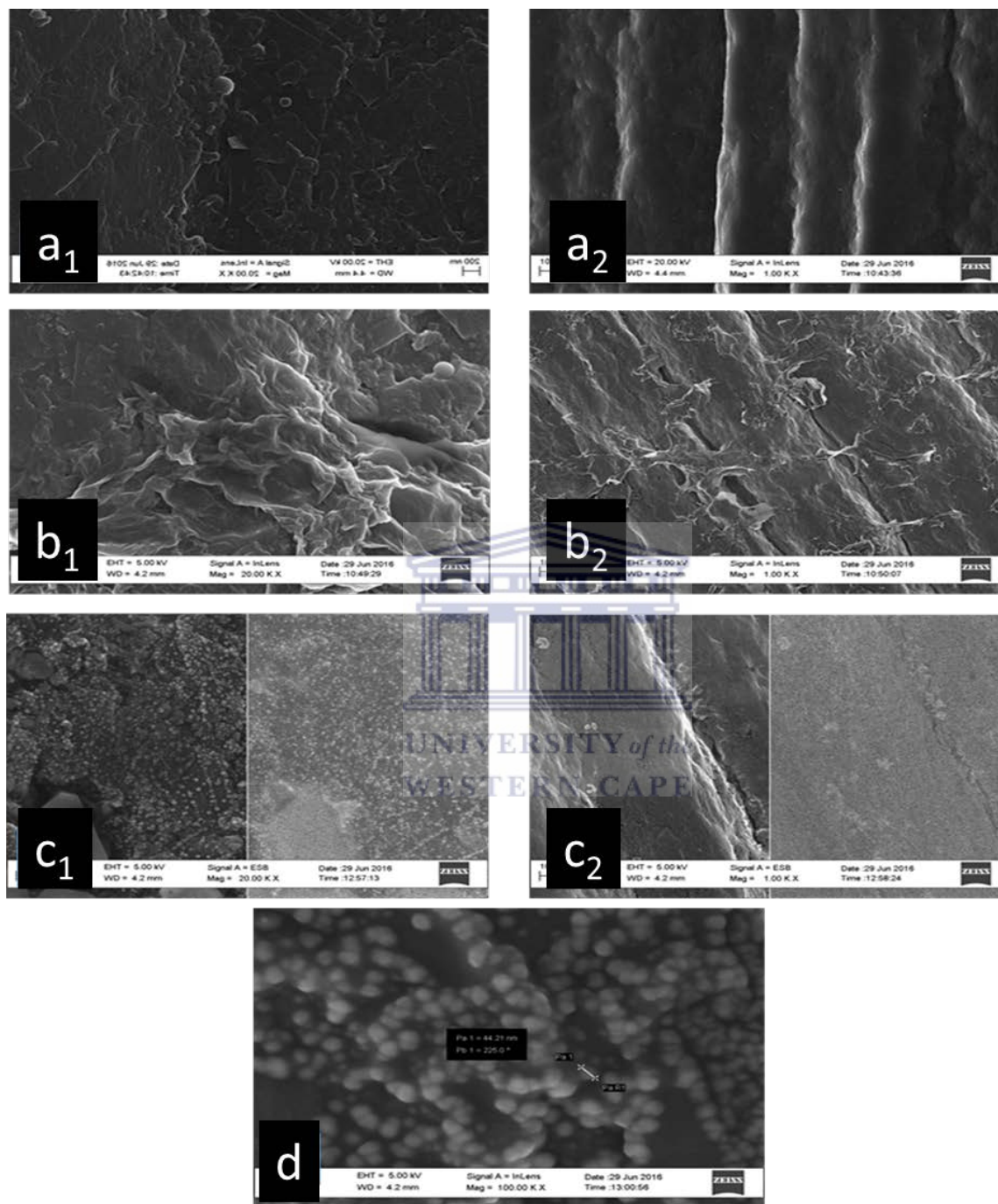
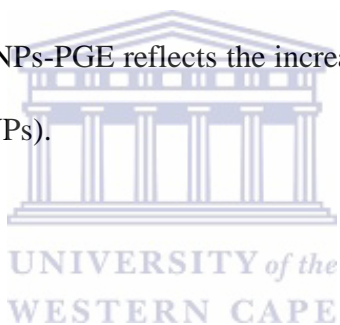


Figure 6.32: HRSEM images of bare PGE (a), EGO-PGE (b), and ERGO-AuNPs-PGE (c) at 20.00 k times magnification (1) and 1000 times magnification (2). HRSEM image of ERGO-AuNPs-PGE at 100.00 k times magnification (d).

6.4.8. Effect of the ERGO-AuNPs nanocomposite surface on electrochemical oxidation of BPA

The electrochemical response of BPA on the ERGO-AuNPs-PGE was evaluated in 0.1 mol L⁻¹ PBS pH 7, containing 50 μM BPA by differential pulse voltammetry (DPV) experiments with amplitude of 100 mV, step potential of 2 mV, and an effective scan rate of 5 mV s⁻¹. The results are presented in Fig 6.33. The DPV voltammetry shows a negative shift for BPA oxidation peak on bare PGE at 542 mV to 461 mV and 416 mV on ERGO-PGE and ERGO-AuNPs-PGE, respectively. Moreover, the BPA oxidation peak on modified ERGO-AuNPs-PGE at 20.2 μA shows a 9 times bigger current than the bare PGE at 2.39 μA. The enhancement in the oxidation current peak of PBA at ERGO-AuNPs-PGE reflects the increase of the electroactive surface area by the formed hybrid (ERGO–AuNPs).



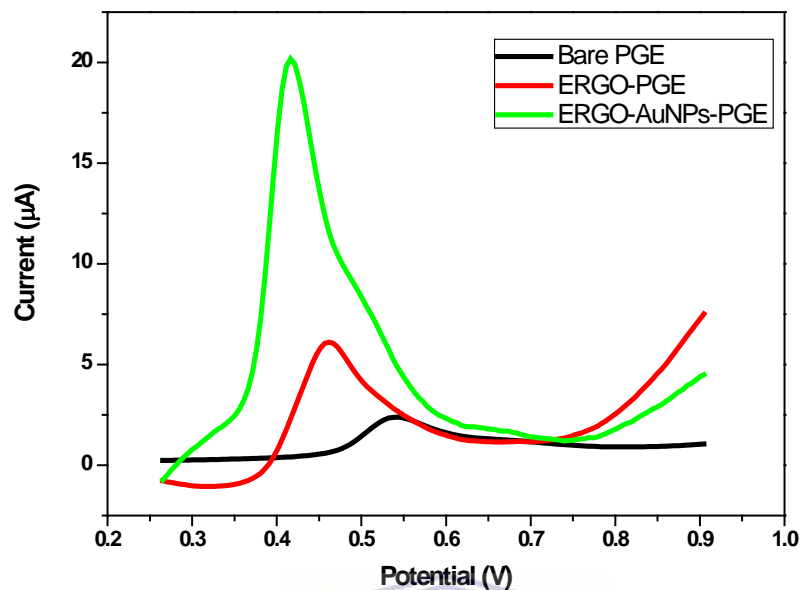
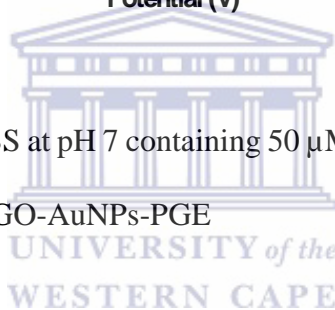


Figure 6.33: DPV of 0.1 molL^{-1} PBS at pH 7 containing $50 \mu\text{M}$ BPA for the electrode (black) bare PGE, (red) ERGO-PGE, (green) ERGO-AuNPs-PGE



6.4.9. Preconcentration time optimization

The pre-concentration time of BPA oxidation was optimized over the time interval from 0 to 120 seconds at ERGO-AuNPs-PGE using differential pulse voltammetry (Figure 6.34). As a longer pre-concentration time allowed for more analyte to be adsorbed onto the electrode, the peak current increased with increasing pre-concentration time. A pre-concentration time of 60 s was used for further measurements.

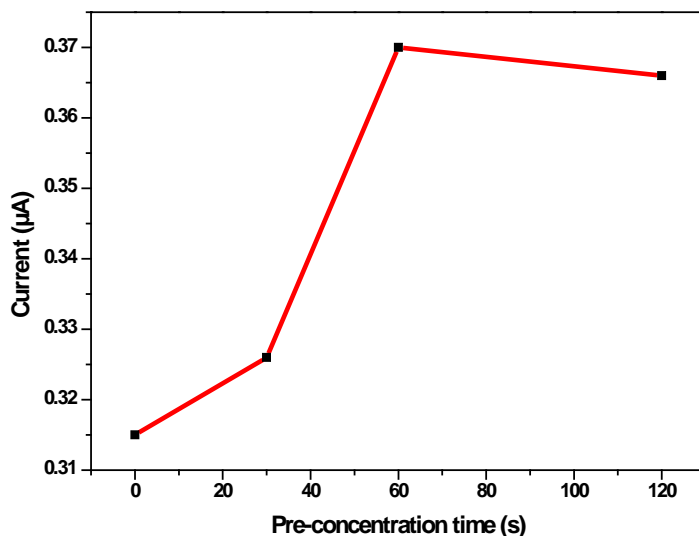
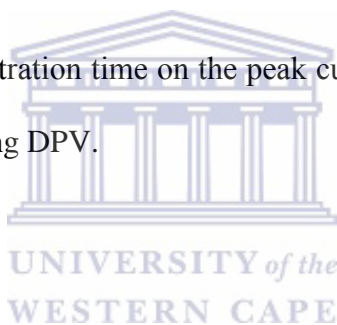


Figure 6.34: Effect of pre-concentration time on the peak current of 5.0 μM BPA in 10 mL 0.1 M PBS at ERGO-AuNPs-PGE using DPV.



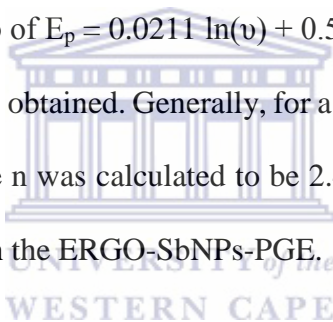
6.4.10. Effect of scan rate on the electrocatalytic oxidation of BPA at ERGO-AuNPs-PGE

Figure 6.35 shows the cyclic voltammograms of BPA at the ERGO-AuNPs-PGE when the scan rate (ν) varies from 10 to 100 mVs^{-1} . As is shown in Fig 6.35 (a), the oxidation peak currents increased linearly in an irreversibly electrode process, indicating that the oxidation of BPA at the ERGO-AuNPs-PGE is adsorption-controlled [52,114,115]. Moreover, not linearity of the plot of the peak current (I_{pa}) against the square root of scan rate ($\nu^{1/2}$), confirms the adsorption-controlled BPA oxidation (Fig 6.35 (d)). The linear regression equations for oxidation peak (I_{pa}) current is: $I_{pa} = 0.478 \nu + 1.64$ with the correlation coefficients of 0.9984 (Fig 6.35 (b)). As

shown in Figure 6.35 (c) there is a linear relationship between the peak potential (E_p) and the natural logarithm of scan rate ($\ln v$) for the ERGO-AuNPs-PGE. As for an irreversibly electrode process, the number of electrons involved in the reaction can be estimated according to the Laviron's equation as follows:

$$E_p = E^0 + (RT/\alpha nF) [\ln (RTk_s/\alpha nF) - \ln v] \quad (\text{Eqn. 6.3})$$

Where α is the electron transfer coefficient, k_s is the standard rate constant of the surface reaction, T is the temperature (298 K here), v is the scan rate, R the gas constant ($8.314 \text{ JK}^{-1}\text{mol}^{-1}$), n is the electron transfer numbers, F the Faraday constant ($96,480 \text{ C mol}^{-1}$) and E^0 the formal redox potential. The αn value can be calculated from the slope of the linear regression equation of the linear plot of E_p with respect to $\ln v$ of $E_p = 0.0211 \ln(v) + 0.515$, $R^2 = 0.998$. $RT/\alpha nF$ was 0.0248 here, then the value of $\alpha n = 1.21$ was obtained. Generally, for a totally irreversible electron transfer, α was assumed to be 0.5. Thus, the n was calculated to be 2.43 showing that two electrons were involved in the oxidation of BPA on the ERGO-SbNPs-PGE.



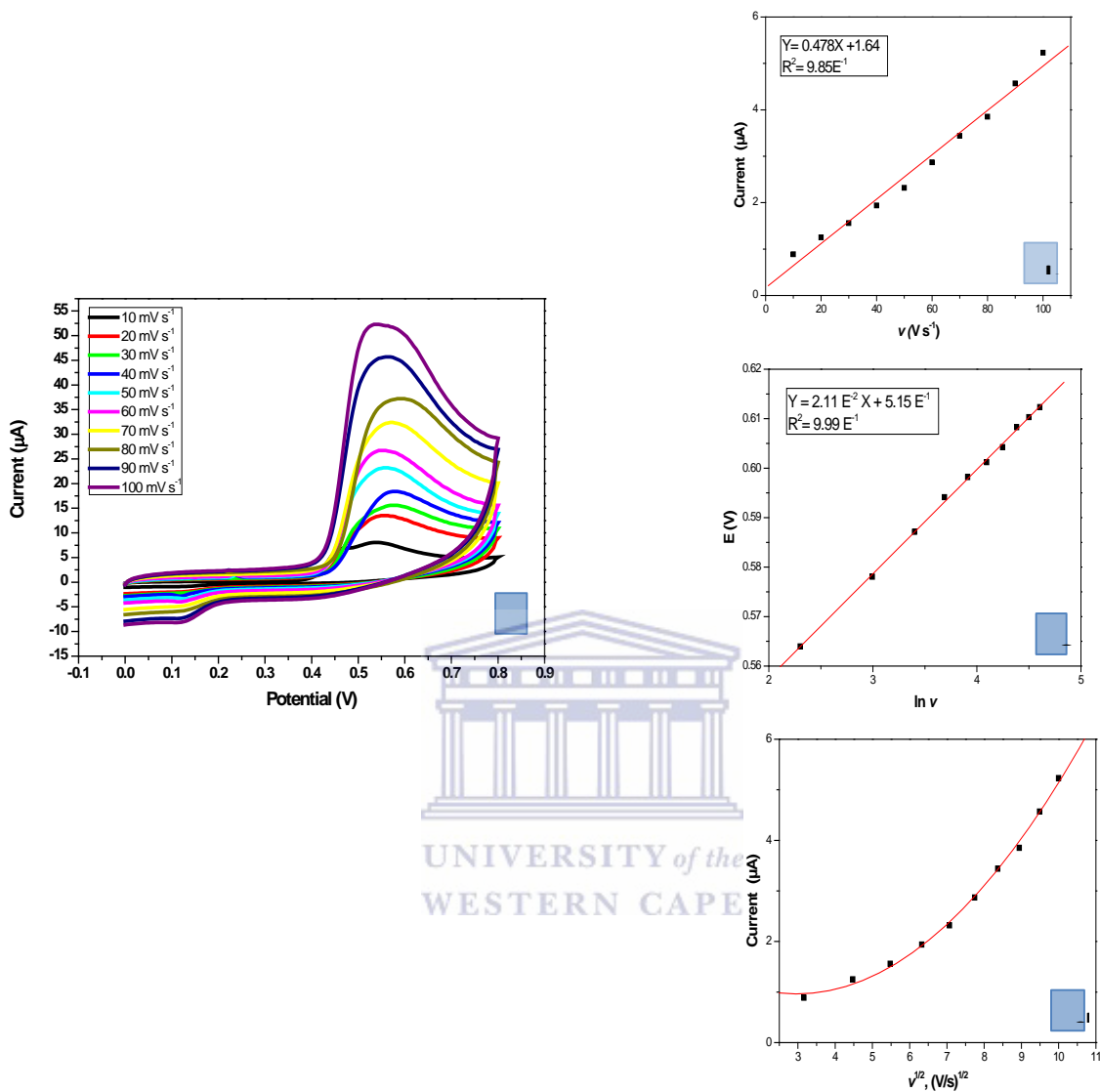


Figure 6.35: (a) Cyclic voltammetric responses of 10 μ M BPA at ERGO-AuNPs-PGE in 0.1 M PBS (pH= 7.0) at scan rates, (inner to outer) 10, 20, 30, 40, 50, 60, 70, 80, 90, 100 mVs⁻¹. (b and d) The plots of peak currents vs scan rate and square root of scan rate, respectively. (c) The variation of peak potential vs $\ln v$.

6.4.11. pH optimization

The influence of pH on the oxidation peak current of BPA on ERGO-AuNPs-PGE was studied with pH ranging from 5 to 10 as shown in Figure 6.36. The oxidation peak at pH 7 showed the highest peak current. Thus pH 7 was selected as the optimum pH electrolyte for subsequent experiments. The linear shifting of the peak potential to more negative values with increasing pH with a slope of -61.24 mV/pH which was close to the theoretical value 57 mV/pH indicates equal number of protons and electrons are involved in the BPA oxidation (a two-electron-two-proton process) [11,86,115].

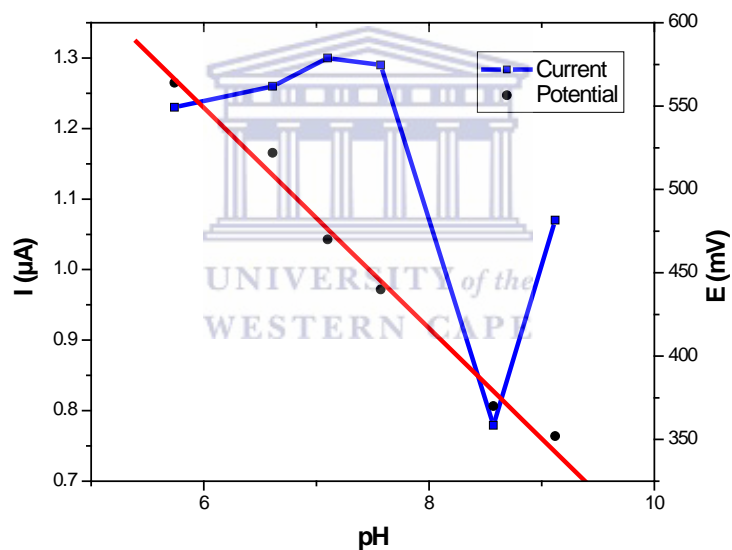


Figure 6.36: Effect of pH on the peak current of $1.0 \mu\text{M}$ BPA in 10 mL 0.1 M PBS at ERGO-AuNPs-PGE using DPV.

6.4.12. Interference studies

The influence of possible interfering molecules for the oxidation measurements of $50 \mu\text{M}$ bisphenol A in the absence and presence of interfering molecules was studied using adsorptive

stripping differential pulse voltammetry (Figure 6.37). The interfering molecules that were examined were as following: 2, 2- Dimethoxyphenol, Potassium Chloride, 4- Hydroxyanisol 4-Methoxyphenol, sodium chloride, 4-cumylphenol. . No electroactivity and change in the voltammetric response was observed for 50 μM BPA in the presence of a two-time excess concentration (100 μM) of electroinactive species except for 4-cumylphenol. The significant increasment observed in the oxidation peak current shows the interfering effect of 4-cumylphenol on response of the electrode towards BPA measurement.



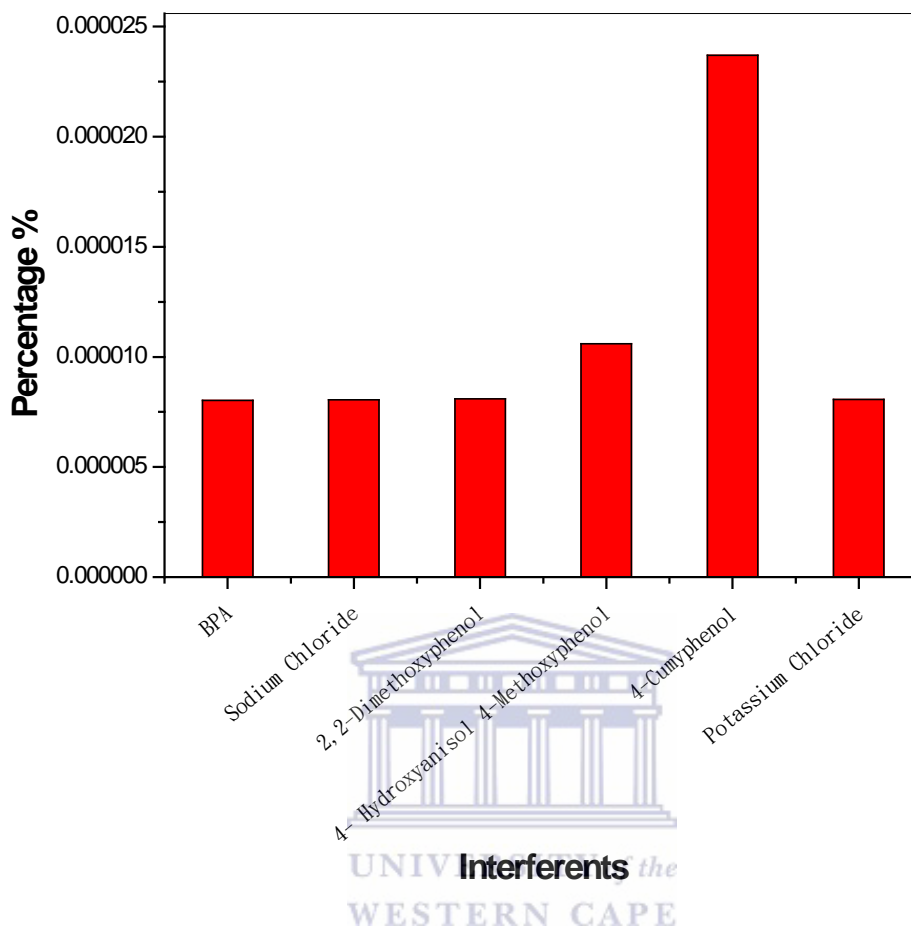


Figure 6.37: Percentages of the oxidation peak current of 50 μM of the BPA in absence and presence of 100 μM 2, 2- Dimethoxyphenol, Potassium Chloride, 4- Hydroxyanisol 4- Methoxyphenol, sodium chloride, 4-cumylphenol.

6.4.13. Detection Limit

A linear relationship between the BPA concentration in the range of 0.4 μM to 5.0 μM and peak current with a correlation coefficient of 0.999 is observed (Figure 6.38). The standard deviation was calculated based on the linear regression equation of the average of calibration curves (n=5) as following:

$$I(\mu\text{A}) = 0.739 (\mu\text{A } \mu\text{mol L}^{-1}) [\text{BPA}] (\mu\text{mol L}^{-1}) + 0.141 (\mu\text{A}) \quad (\text{Eqn. 6.4})$$

Detection limit for biphenol A with ERGO-AuNPs-PGE was determined using following equation:

$$\text{D.L.} = 3\sigma/\text{slope} \quad (\text{Eqn. 6.5})$$

Where,

D.L., is the limit of detection

3σ , is three times the standard deviation of the blanks

Slope, is the gradient (slope) of the calibration curve

The detection limit was found to be $0.062 \mu\text{M}$ based on ten replications of the electrode's response in the blank solutions.

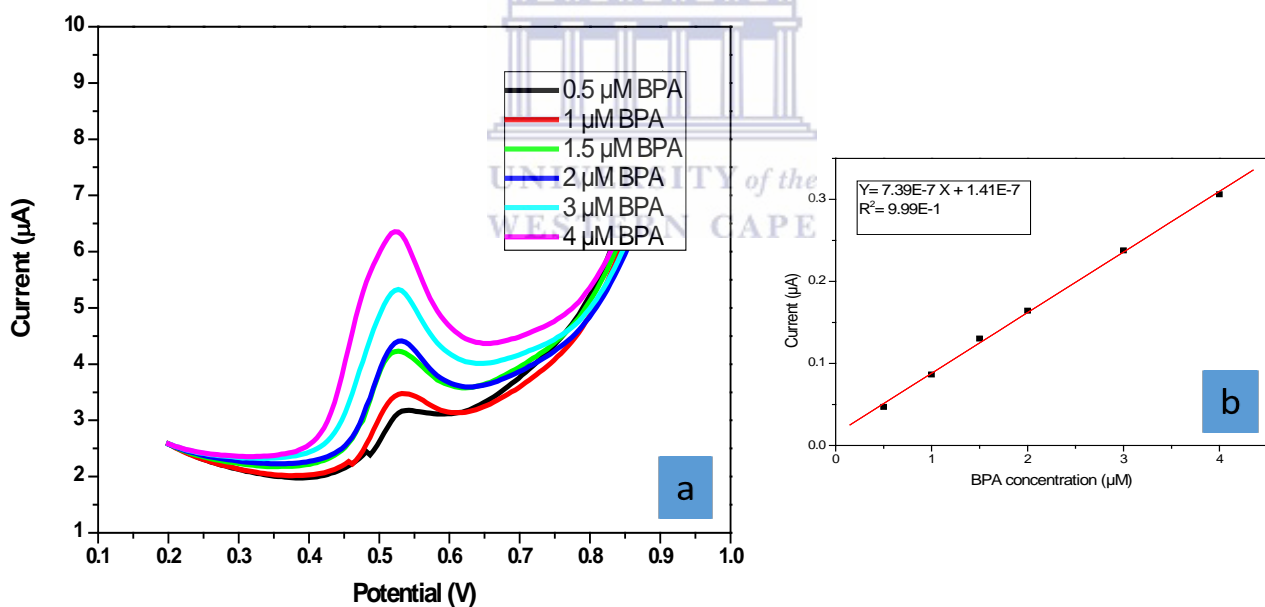


Figure 6.38: DPV voltammograms for ERGO-AuNPs-PGE with the optimised parameters (a). The BPA concentrations range from $0.4 \mu\text{mol L}^{-1}$ to $5.0 \mu\text{mol L}^{-1}$. Linear dependence of the peak current with BPA concentration (b).

The calculated detection limit is comparable to those reported in the literature. The analytical parameters obtained in this study and those reported previously is shown in Table 6.2. However lower detection limits have been found in the reported literature but fouling problem as the main challenge for the determination of BPA [11], [12], [54] is eliminated using the single used ERGO-AuNPs-PGE.

Table 6.2. Comparison of the proposed method with some of the previously sensors.

Electrode	Linear range (μM)	Detection limit (μM)	Reference
GCE-MWCNT-AuNPs	0.02-0.2	0.0075	[38]
ssDNA/SWCNT/Au	1-3.8	0.045	[53]
PAMAM-AuNPs-NF/GCE	0.001-0.0103	0.005	[52]
AuNPs/GR based aptasenor	0.001-10	0.005	[10]
RGOM-GCE	0.01-200	0.004	[115]
GC/MWCNTs	4-8	0.084	[54]
ERGO-AuNPs-PGE	0.4-5.0	0.062	This study

* GCE-MWCNT-AuNPs: nanotubes-gold nanoparticles modified glassy carbon electrode, ssDNA/SWCNT/Au: single-stranded DNA (ssDNA) wrapped CNTs on a gold substrate, PAMAM-AuNPs-NF/GCE: glassy carbon electrode modified with gold nanoparticles, silk fibroin, and PAMAM dendrimers, AuNPs/GR based aptasenor: An electrochemical aptasensor based on gold nanoparticles dotted graphene modified glassy carbon electrode for, RGOM-GCE: graphene/melamine nanoparticle-modified glassy carbon electrode, GC/MWCNTs: glassy carbon electrode modified with multi wall carbon nanotubes.

6.4.14. Analytical application of ERGO-AuNPs–PGE

The ERGO-AuNPs-PGE was used to determine bisphenol A in real water samples using differential pulse adsorptive stripping voltammetry. Known concentration of bisphenol A was used to spiked 10 mL portion of tap water sample prepared as described in the experimental and determined using standard addition method (Figure 6.39). Recovery percentage of bisphenol A determination performed three times in tap water sample solutions spiked with 0.2 μM BPA values in the range of 96.98 % to 103.5 % which found to be satisfactory. The range of relative standard deviation of 1.3- 4 % was calculated for the oxidation peak of BPA in tap water samples showing less than 5 % error in the quantification of BPA in tap water sample using the ERGO-AuNPs-PGE.

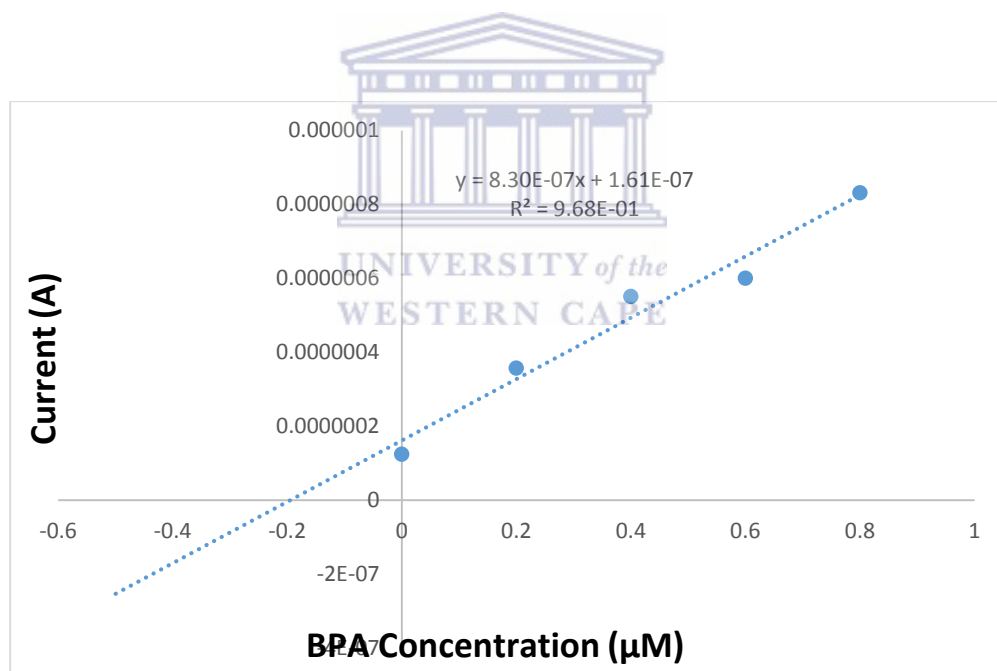


Figure 6.39: Linear dependence of the peak currents and BPA concentrations. Tap water sample spiked with 0.2 μM BPA and 0.2 μM BPA was added three times.

6.5. Conclusion

Modification of pencil graphite electrodes with a reduced graphene oxide metal nanocomposite for the detection of bisphenol A by differential pulse adsorptive voltammetry was characterized

electrochemically and microscopically. Improved detection limits were found to be comparable to other known carbon-based electrodes and below USEPA standards as well as accurate detection of BPA in tap water samples with a 5% error.



CHAPTER SEVEN

Conclusions and Future Work

This study demonstrates the need of finding sensitive and inexpensive techniques for the determination of bisphenol A by differential pulse adsorptive stripping voltammetry and clarifies the use of graphene-metal nanocomposite as a good coating material. A sensitive electrochemical sensor for determining bisphenol A was prepared based on the direct electrochemical reduction of colloidal graphene oxide metal nanocomposite at pencil graphite electrodes with the sensitivity comparable to that of the glassy carbon electrodes.

The pencil graphite electrode modified with graphene-antimony nanocomposite showed an improved detection limit of bisphenol A comparable to other known pencil graphite electrodes. The enhanced sensing capabilities of reduced graphene oxide antimony nanoparticles pencil graphite electrode was proved by the accurate detection of bisphenol A in tap water samples with a 5% error.

The assessment of the analytical application of the reduced graphene oxide gold nanoparticles pencil graphite electrode was conducted by recovery studies and real sample analysis with a low detection limit below the USEPA standard of BPA.

The future work includes the use of pencil graphite electrode modified with various graphene-metal nanocomposites to existing green approach. The electroanalytical use of graphene-metal nanocomposite pencil graphite electrodes has been encouraged based on the achieved results.

In future, the use of pencil graphite electrode as a substrate that offer good results comparable to common electrode substrates could be investigated for a wide range of applications. The pencil graphite substrate could be used for future studies as a low cost and disposable electrode.

Bibliography

- [1] J.J. Heindel, S. Jobling, K.A. Kidd, R.T. Zoeller, Endocrine Disrupting Chemicals - 2012, 2012.
- [2] T. Doshi, S.S. Mehta, V. Dighe, N. Balasinor, G. Vanage, Hypermethylation of estrogen receptor promoter region in adult testis of rats exposed neonatally to bisphenol A, *Toxicology*. 289 (2011) 74–82. doi:10.1016/j.tox.2011.07.011.
- [3] U.S.E.P. Agency, U.S. Environmental Protection Agency 3/29/2010, (2011) 1–22.
- [4] G. Gatidou, N.S. Thomaidis, A.S. Stasinakis, T.D. Lekkas, Simultaneous determination of the endocrine disrupting compounds nonylphenol, nonylphenol ethoxylates, triclosan and bisphenol A in wastewater and sewage sludge by gas chromatography-mass spectrometry, *J. Chromatogr. A*. 1138 (2007) 32–41. doi:10.1016/j.chroma.2006.10.037.
- [5] J. Ou, L. Hu, L. Hu, X. Li, H. Zou, Determination of phenolic compounds in river water with on-line coupling bisphenol A imprinted monolithic precolumn with high performance liquid chromatography, *Talanta*. 69 (2006) 1001–1006. doi:10.1016/j.talanta.2005.12.003.
- [6] H. Fromme, T. Kuchler, T. Otto, K. Pilz, J. Müller, A. Wenzel, Occurrence of phthalates and bisphenol A and F in the environment, *Water Res.* 36 (2002) 1429–1438. doi:10.1016/S0043-1354(01)00367-0.
- [7] EFSA, Scientific Opinion on the risks to public health related to the presence of nickel in food and drinking water, *EFSA J.* 13 (2015) 4002. doi:10.2903/j.efsa.2015.4002.
- [8] J.H. Kang, F. Kondo, Y. Katayama, Human exposure to bisphenol A, *Toxicology*. 226 (2006) 79–89. doi:10.1016/j.tox.2006.06.009.
- [9] P. Smad, M.L. Slattery, J. Herrick, K. Curtin, W. Samowitz, R.K. Wolff, B.J. Caan, D.

- Duggan, J.D. Potter, U. Peters, NIH Public Access, 70 (2011) 1479–1485.
doi:10.1158/0008-5472.CAN-08-1792.Increased.
- [10] L. Zhou, J. Wang, D. Li, Y. Li, An electrochemical aptasensor based on gold nanoparticles dotted graphene modified glassy carbon electrode for label-free detection of bisphenol A in milk samples, *FOOD Chem.* 162 (2014) 34–40.
doi:10.1016/j.foodchem.2014.04.058.
- [11] A. Özcan, Synergistic Effect of Lithium Perchlorate and Sodium Hydroxide in the Preparation of Electrochemically Treated Pencil Graphite Electrodes for Selective and Sensitive Bisphenol A Detection in Water Samples, *Electroanalysis.* 26 (2014) 1631–1639. doi:10.1002/elan.201400082.
- [12] B. Sebez, B. Ogorevc, S.B. Hocevar, M. Veber, *Analytica Chimica Acta* Functioning of antimony film electrode in acid media under cyclic and anodic stripping voltammetry conditions, *Anal. Chim. Acta.* 785 (2013) 43–49. doi:10.1016/j.aca.2013.04.051.
- [13] T. Ndlovu, O.A. Arotiba, S. Sampath, R.W. Krause, B.B. Mamba, An exfoliated graphite-based bisphenol a electrochemical sensor, *Sensors (Switzerland).* 12 (2012) 11601–11611. doi:10.3390/s120911601.
- [14] X. Niu, W. Yang, G. Wang, J. Ren, H. Guo, J. Gao, *Electrochimica Acta* A novel electrochemical sensor of bisphenol A based on stacked graphene nanofibers / gold nanoparticles composite modified glassy carbon electrode, *Electrochim. Acta.* 98 (2013) 167–175. doi:10.1016/j.electacta.2013.03.064.
- [15] J. Wang, *ANALYTICAL ELECTROCHEMISTRY*, Third, John Wiley & Sons, 2006.
- [16] S.B. Hocevar, S. Ivan, B. Ogorevc, K. Vytr, Antimony Film Electrode for Electrochemical Stripping Analysis, 79 (2007) 8639–8643. doi:10.1021/ac070478m.

- [17] J. Wang, A. Kawde, E. Sahlin, R. September, A. September, Renewable pencil electrodes for highly sensitive stripping potentiometric measurements of DNA and RNA, (2000) 5–7.
- [18] K. Pokpas, S. Zbeda, N. Jahed, N. Mohamed, P.G. Baker, E.I.I. Sensorlab, Electrochemically Reduced Graphene Oxide Pencil-Graphite in situ Plated Bismuth-film Electrode for the Determination of Trace Metals by Anodic Stripping Voltammetry, *Int. J. Electrochem. Sci.* 9 (2014) 736–759. www.electrochemsci.org (accessed September 14, 2016).
- [19] K. Pokpas, N. Jahed, O. Tovide, P.G. Baker, E.I. Iwuoha, Nafion-graphene nanocomposite in situ plated bismuth-film electrodes on pencil graphite substrates for the determination of trace heavy metals by anodic stripping voltammetry, *Int. J. Electrochem. Sci.* 9 (2014) 5092–5115.
- [20] S. Zbeda, K. Pokpas, S. Titinchi, N. Jahed, P.G. Baker, E.I. Iwuoha, Few-layer Binder Free Graphene Modified Mercury Film Electrode for Trace Metal Analysis by Square Wave Anodic Stripping Voltammetry, 8 (2013) 11125–11141.
- [21] H. Yang, C. Shan, F. Li, Q. Zhang, D. Han, L. Niu, Convenient preparation of tunably loaded chemically converted graphene oxide / epoxy resin nanocomposites from graphene oxide sheets through two-phase extraction †, (2009) 8856–8860. doi:10.1039/b915228h.
- [22] J. Huang, Y. Liu, H. Hou, T. You, Biosensors and Bioelectronics Simultaneous electrochemical determination of dopamine , uric acid and ascorbic acid using palladium nanoparticle-loaded carbon nanofibers modified electrode, 24 (2008) 632–637. doi:10.1016/j.bios.2008.06.011.
- [23] Y. Song, K. Cui, L. Wang, S. Chen, The electrodeposition of Ag nanoparticles on a type I collagen-modified glassy a hydrogen peroxide sensor, (2009). doi:10.1088/0957-

4484/20/10/105501.

- [24] J. Li, S. Guo, Y. Zhai, E. Wang, *Analytica Chimica Acta* High-sensitivity determination of lead and cadmium based on the Nafion-graphene composite film, 649 (2009) 196–201. doi:10.1016/j.aca.2009.07.030.
- [25] S. Otlés, *Electroanalytical Techniques and Instrumentation in Food Analysis*, *Handb. Food Anal. Instruments*. (2008).
- [26] P. Kissinger and W. Heineman, No Title, *Laboratory Tech. Electroanal. Chem.* (1996).
- [27] C. Zoski, *Handbook of Electrochemistry*, Elsevier. (2007).
- [28] L.. Bard, A.J.; Faulkner, No Title, *Electrochem. Methods Fundam. Appl.* (2000).
- [29] J. Wang, *Stripping Analysis-Principles, Instrumentation and Application*, Inc. (1985).
- [30] P. Monk, No Title, *Fundam. Electro-Analytical Chem.* (2001).
- [31] J.P. Franke; R.A. De Zeeuw, *Differential Pulse Anodic Stripping Voltammetry as a Rapid Screening Technique for Heavy Metals Intoxications*, *Arch Toxicol.* 37 (1976) 47–55.
- [32] P.A. Eric, B. Charlotte, *Stripping Voltammetry for the determination of trace metal speciation and in-situ measurements of trace metal distribution in marine waters*, *Anal. Chim. Acta.* 400 (1999) 381–397.
- [33] D.W.M. Arrigan, *Voltammetric Determination of Trace Metals and Organics after Accumulation at Modified Electrodes*, 11 (1994) 1953–1966.
- [34] S. Gumaa, A. Zbeda, *Multilayer graphene modified metal film electrodes for the determination of trace metals by anodic stripping voltammetry*, (2013).
- [35] S. A. Ozkan, *Principles and Techniques of Electrochemical Stripping Methods for Pharmaceutically Active Compounds in Dosage Forms and Biological Samples*, *Curr. Pharm. Anal.* 5 (2009) 127–143.

- [36] K. Robert, K. Miloslav, Adsorptive stripping in trace analysis, *Pure Appl. Chem.* (1989) 97–112.
- [37] J. Li, D. Kuang, Y. Feng, Voltammetric determination of bisphenol A in food package by a glassy carbon electrode modified with carboxylated multi-walled carbon nanotubes, (2011) 379–386. doi:10.1007/s00604-010-0512-0.
- [38] X. Tu, L. Yan, X. Luo, S. Luo, Electroanalysis of Bisphenol A at a Multiwalled Carbon Nanotubes-gold Nanoparticles Modified Glassy Carbon Electrode, (2009) 2491–2494. doi:10.1002/elan.200900195.
- [39] W. Huang, Voltammetric Determination of Bisphenol A Using a Carbon Paste Electrode Based on the Enhancement Effect of Cetyltrimethylammonium Bromide (CTAB), *Bull. Korean Chem. Soc.* 26 (2005) 1560–1564.
- [40] J.R. Rochester, Bisphenol A and human health : A review of the literature, *Reprod. Toxicol.* 42 (2013) 132–155. doi:10.1016/j.reprotox.2013.08.008.
- [41] X. Wang, H. Zeng, Y. Wei, J. Lin, A reversible fluorescence sensor based on insoluble β -cyclodextrin polymer for direct determination of bisphenol A (BPA), 114 (2006) 565–572. doi:10.1016/j.snb.2005.06.020.
- [42] A. García-prieto, M.L. Lunar, S. Rubio, D. Pérez-bendito, Determination of urinary bisphenol A by coacervative microextraction and liquid chromatography – fluorescence detection, 0 (2008) 19–27. doi:10.1016/j.aca.2008.09.060.
- [43] X. Wang, H. Zeng, L. Zhao, J. Lin, Selective determination of bisphenol A (BPA) in water by a reversible fluorescence sensor using pyrene / dimethyl β -cyclodextrin complex, 556 (2006) 313–318. doi:10.1016/j.aca.2005.09.060.

- [44] Y. Ji, J. Yin, Z. Xu, C. Zhao, H. Huang, H. Zhang, C. Wang, determination of bisphenol A in environmental water and milk samples Preparation of magnetic molecularly imprinted polymer for rapid determination of bisphenol A in environmental water and milk samples, *Anal Bioanal Chem.* 395 (2009) 1125–1133. doi:10.1007/s00216-009-3020-5.
- [45] M.R. Hadjmohammadi, Determination of bisphenol A in Iranian packaged milk by solid-phase extraction and HPLC, (2010) 501–506. doi:10.1007/s00706-010-0297-1.
- [46] E.M. Malone, C.T. Elliott, D.G. Kennedy, L. Regan, Rapid confirmatory method for the determination of sixteen synthetic growth promoters and bisphenol A in bovine milk using dispersive solid-phase extraction and liquid chromatography – tandem mass spectrometry, *J. Chromatogr. B.* 878 (2010) 1077–1084. doi:10.1016/j.jchromb.2010.03.012.
- [47] R. Zhao, X. Wang, Highly sensitive determination of tetrabromobisphenol A and bisphenol A in environmental water samples by solid-phase extraction and liquid chromatography- tandem mass spectrometry, (2010) 1652–1657. doi:10.1002/jssc.201000010.
- [48] E. Herrero, R. Carabias, E. Rodr, *Analytica Chimica Acta* Use of a bisphenol-A imprinted polymer as a selective sorbent for the determination of phenols and phenoxyacids in honey by liquid chromatography with diode array and tandem mass spectrometric detection, 650 (2009) 195–201. doi:10.1016/j.aca.2009.07.043.
- [49] M. Zhao, Y. Li, Z. Guo, X. Zhang, A new competitive enzyme-linked immunosorbent assay (ELISA) for determination of estrogenic bisphenols, 57 (2002) 1205–1210.
- [50] X. Jin, G. Jiang, G. Huang, Determination of 4- tert -octylphenol , 4-nonylphenol and bisphenol A in surface waters from the Haihe River in Tianjin by gas chromatography – mass spectrometry with selected ion monitoring, 56 (2004) 1113–1119.

- doi:10.1016/j.chemosphere.2004.04.052.
- [51] C. Sánchez-brunete, E. Miguel, J.L. Tadeo, Determination of tetrabromobisphenol-A , tetrachlorobisphenol-A and bisphenol-A in soil by ultrasonic assisted extraction and gas chromatography – mass spectrometry, 1216 (2009) 5497–5503.
doi:10.1016/j.chroma.2009.05.065.
- [52] H. Yin, Y. Zhou, S. Ai, R. Han, Electrochemical behavior of bisphenol A at glassy carbon electrode modified with gold nanoparticles , silk fibroin , and PAMAM dendrimers, (2010) 99–105. doi:10.1007/s00604-010-0396-z.
- [53] F.C. Moraes, T.A. Silva, I. Cesarino, S.A.S. MacHado, Effect of the surface organization with carbon nanotubes on the electrochemical detection of bisphenol A, Sensors Actuators, B Chem. 177 (2013) 14–18. doi:10.1016/j.snb.2012.10.128.
- [54] L.A. Goulart, F.C. De Moraes, L.H. Mascaro, Influence of the different carbon nanotubes on the development of electrochemical sensors for bisphenol A, Mater. Sci. Eng. C. 58 (2016) 768–773. doi:10.1016/j.msec.2015.09.073.
- [55] S. Poorahong, C. Thammakhet, P. Thavarungkul, W. Limbut, A. Numnuam, P. Kanatharana, Amperometric sensor for detection of bisphenol A using a pencil graphite electrode modified with polyaniline nanorods and multiwalled carbon nanotubes, Microchim. Acta. 176 (2012) 91–99. doi:10.1007/s00604-011-0698-9.
- [56] A.R. Reserved, Introduction to Nanoscience and Nanotechnology : A Workbook, (2005).
- [57] K. Klabunde, R. Richards, Nanoscale Materials in Chemistry, Inc. (2009).
- [58] T. Takagahara, K. Takeda, Theory of the Quantum Confinement Effect on Excitons in Quantum Dots of Indirect-gap Materials, Phys.Rev. B. 46 (1992) 15578–15581.
- [59] O.Arsenault, A Chemical Approach to Nanomaterials, Cambridge R. Soc. Chem. (2005).

- [60] B. Pollard, Growing Graphene via Chemical Vapor Deposition, Dep. Physics, Pomona Coll. (2011).
- [61] A.C. Neto, F. Guinea, N.M. Peres, Drawing conclusions from graphene, Phys. World. (2006). doi:10.1088/2058-7058/19/11/34.
- [62] J. Bunch, S. Verbridge, J. Alden, A. van der Zande, J. Parpia, H. Craighead, P. McEuen, Impermeable Atomic Membranes from Graphene Sheets, Nano Lett. 8 (2008) 2458–2462.
- [63] A.G. and K. Novoselov, The Rise of Graphene, Nat. Mater. 6 (2007) 183–191.
- [64] D. Demetriades, A. Economou, A. Voulgaropoulos, A study of pencil-lead bismuth-film electrodes for the determination of trace metals by anodic stripping voltammetry, 519 (2004) 167–172. doi:10.1016/j.aca.2004.05.008.
- [65] J.M. Raimond, M. Brune, Q. Compton, F. De Martini, C. Monroe, Electric Field Effect in Atomically Thin Carbon Films, 306 (2004) 666–670.
- [66] C. Willemse, K. Tlhomelang, N. Jahed, P. Baker, E. Iwuoha, Metallo-Graphene Nanocomposite Electrocatalytic Platform for the Determination of Toxic Metal Ions, Sensors. 11 (2011) 3970–3987.
- [67] B. Partoens, F.M. Peeters, From graphene to graphite: Electronic structure around the K point., Phys. Rev. B. 74 (2006) 075404. doi:10.1103/PhysRevB.74.075404.
- [68] S. Arar, Everything You Need to Know About the Future of Graphene, All About Circuits. (2016). <https://www.allaboutcircuits.com/news/everything-you-need-to-know-about-the-future-of-graphene/>.
- [69] C. Schonberger, Bandstructure of Graphene and Carbon Nanotubes: Exercise in Condensed Matter Physics, n.d.
- [70] O. Kharisov, Graphenes, One of the hottest Areas in the Nanotechnology: Attention of

- Chemists is Needed, *Open Inorg. Chem. J.* 2 (2008) 39–49.
- [71] L.A. Falkovsky, Optical properties of graphene and IV-VI semiconductors, *Phys.-Usp.* 51 (2008) 887. doi:10.1070/PU2008v051n09ABEH006625.
- [72] B. Brodie, Sur le poids atomique du graphite, *An, Chim. Phys.* 59 (1860) 466–472.
- [73] W.S. Hummers, R.E. Offeman, Preparation of Graphitic Oxide, 1958.
<https://pubs.acs.org/sharingguidelines> (accessed August 21, 2018).
- [74] L. Staudenmaier, Verfahren zur darstellung der graphitsaure, *Ber. Dtsch. Chem Ges.* 31 (1898) 1481–1499.
- [75] A. Reina, S. Thiele, X. Jia, S. Bhaviripudi, S. Mildred, Growth of Large-area Single- and Bi-layer Graphene by Controlled Carbon Precipitation on Polycrystalline Ni Surfaces, (n.d.) 1–27.
- [76] H. Jin, J. Meyer, S. Roth, Growth and properties of few-layer graphene prepared by chemical vapor deposition, 8 (2009) 0–6. doi:10.1016/j.carbon.2009.11.030.
- [77] M. Voutilainen, E.T. Seppälä, P. Pasanen, M. Oksanen, Graphene and Carbon Nanotube Applications in Mobile Devices, 59 (2012) 2876–2887.
- [78] N. Shang, P. Wang, Platinum Integrated Graphene for Methanol Fuel Cells, (2010) 15837–15841.
- [79] P. Reunchan, S. Jhi, Metal-dispersed Porous Graphene for Hydrogen Storage, *Appl. Phys. Lett.* 98 (2011) 093103-093103-3.
- [80] H. Wang, L. Cui, Y. Yang, H.S. Casalongue, Mn₃O₄ - Graphene Hybrid as a High-Capacity Anode Material for Lithium Ion, (2010) 13978–13980.
- [81] Y. Shao, J. Wang, H. Wu, J. Liu, I.A. Aksay, Y. Lin, Graphene Based Electrochemical Sensors and Biosensors : A Review, (2010) 1027–1036. doi:10.1002/elan.200900571.

- [82] S. Guo, E. Wang, Synthesis and electrochemical applications of gold nanoparticles, 598 (2007) 181–192. doi:10.1016/j.aca.2007.07.054.
- [83] M. Begon, A.C. Garcia, Metal-Nanoparticles Based Electroanalysis, (2002) 1225–1235.
- [84] T.M. Day, P.R. Unwin, N.R. Wilson, J. V Macpherson, Electrochemical Templating of Metal Nanoparticles and Nanowires on Single-Walled Carbon Nanotube Networks, (2005) 10639–10647.
- [85] I. Cesarino, F.H. Cincotto, S.A.S. Machado, A synergistic combination of reduced graphene oxide and antimony nanoparticles for estriol hormone detection, Sensors Actuators, B Chem. 210 (2015) 453–459. doi:10.1016/j.snb.2015.01.013.
- [86] B. Ntsendwana, B.B. Mamba, S. Sampath, O.A. Arotiba, Electrochemical Detection of Bisphenol A Using Graphene- Modified Glassy Carbon Electrode, Int. J. Electrochem. Sci. 7 (2012) 3501–3512.
- [87] F.C. Moraes, I. Cesarino, V. Cesarino, L.H. Mascaro, S.A.S. MacHado, Carbon nanotubes modified with antimony nanoparticles: A novel material for electrochemical sensing, Electrochim. Acta. 85 (2012) 560–565. doi:10.1016/j.electacta.2012.08.123.
- [88] E. Svobodová, L. Baldrianová, S.B. Ho, I. Švancara, Electrochemical Stripping Analysis of Selected Heavy Metals at Antimony Trioxide-Modified Carbon Paste Electrode, 7 (2012) 197–210.
- [89] A. Erdem, H. Karadeniz, A. Caliskan, Single-Walled Carbon Nanotubes Modified Graphite Electrodes for Electrochemical Monitoring of Nucleic Acids and Biomolecular Interactions, (2009) 464–471. doi:10.1002/elan.200804422.
- [90] M. Muti, S. Sharma, A. Erdem, Electrochemical Monitoring of Nucleic Acid Hybridization by Single-Use Graphene Oxide-Based Sensor, (2011) 272–279.

doi:10.1002/elan.201000425.

- [91] L. Chen, Y. Tang, K. Wang, C. Liu, S. Luo, *Electrochemistry Communications Direct* electrodeposition of reduced graphene oxide on glassy carbon electrode and its electrochemical application, *Electrochem. Commun.* 13 (2011) 133–137.
doi:10.1016/j.elecom.2010.11.033.
- [92] G. Nanosheets, H. Guo, X. Wang, Q. Qian, F. Wang, X. Xia, *ARTICLE A Green Approach to the Synthesis of*, 3 (2009) 2653–2659.
- [93] C. Su, A. Lu, Y. Xu, F. Chen, A.N. Khlobystov, L. Li, *High-Quality Thin Graphene Films from Fast Electrochemical Exfoliation*, (2011) 2332–2339. doi:10.1021/nn200025p.
- [94] Y. Shao, J. Wang, M. Engelhard, C. Wang, Y. Lin, *Facile and controllable electrochemical reduction of graphene oxide and its applications †*, (2010).
doi:10.1039/b917975e.
- [95] *Analytical I, Characterization of Materials by FT-IR*, n.d.
- [96] P. Griffiths, *Fourier Transform Infrared Spectrometry*, *Science* (80-.). 222 (1983) 297–302.
- [97] W. Zachariasen, *A General Theory of X-Ray Diffraction in Crystals*, *Acta Cryst.* 23 (1967) 558–564.
- [98] N. Colthup, *Introduction to Infrared and Raman Spectroscopy*, Elsevier. (1990).
- [99] C. Bosch-Navarro, E. Coronado, C. Martí-Gastaldo, J.F. Sánchez-Royoc, M.G. Gómezc, *Influence of the pH on the synthesis of reduced graphene oxide under hydrothermal conditions*, *Nanoscale*. (2012).
- [100] D. Marcano, D. Kosynkin, J. Berlin, A. Sinitskii, Z. Sun, A. Slesarev, L. Alemany, W. Lu, J. Tour, *Improved Synthesis of Graphene Oxide*, *ACS Nano*. 4 (2010) 4806–4814.

- [101] W. Chen, L. Yan, Preparation of Graphene by a Low-temperature Thermal Reduction at Atmosphere Pressure, *Nanoscale*. 2 (2010) 559–563.
- [102] A. Bourlinos, D. Gournis, D. Petridis, T. Szabo, A. Szeri, I. Dekany, Graphite Oxide: Chemical Reduction to Graphite and Surface Modification with Primary Aliphatic Amines and Amino Acids, *Langmuir*. 19 (2003) 6050–6055.
- [103] S. Stankovich, D. Dikin, R. Piner, K. Kohlhaas, A. Kleinhammes, Y. Jia, Y. Wu, S. Nguyen, R. Ruoff, Synthesis of Graphene-based Nanosheers via Chemical Reduction of Exfoliated Graphite Oxide, *Carbon N. Y.* (2007) 1558–1565.
- [104] Y. Zhu, S. Murali, W. Cai, X. Li, J.W. Suk, J.R. Potts, R.S. Ruoff, Graphene and graphene oxide: Synthesis, properties, and applications, *Adv. Mater.* (2010).
doi:10.1002/adma.201001068.
- [105] F.Y. Ban, S.R. Majid, N.M. Huang, H.N. Lim, Graphene Oxide and Its Electrochemical Performance, 7 (2012) 4345–4351.
- [106] M. Del Prado Lavin-Lopez, A. Romero, J. Garrido, L. Sanchez-Silva, J.J. Valverde, Influence of Different Improved Hummers Method Modifications on the Characteristics of Graphite Oxide in Order to Make a More Easily Scalable Method, (2016).
doi:10.1021/acs.iecr.6b03533.
- [107] R. Paper, *Electrochemical Biosensors - Sensor Principles and Architectures*, (2008) 1400–1458.
- [108] V. Determination, P. Ii, P. Clara, J. Bastos-arrieta, N. Serrano, D. Manuel, Ag Nanoparticles Drop-Casting Modification of, (n.d.). doi:10.3390/s17061458.
- [109] E. Casero, A.M. Parra-Alfambra, M.D. Petit-Domínguez, F. Pariente, E. Lorenzo, C. Alonso, Differentiation between graphene oxide and reduced graphene by electrochemical

- impedance spectroscopy (EIS), *Electrochem. Commun.* 20 (2012) 63–66.
doi:10.1016/j.elecom.2012.04.002.
- [110] B. Devadas, M. Rajkumar, Electrochemically reduced graphene oxide/neodymium hexacyanoferrate modified electrodes for the electrochemical detection of paracetamol, *Int. J. Electrochem. Sci.* 7 (2012) 3339–3349.
<http://www.electrochemsci.org/papers/vol7/7043339.pdf>.
- [111] S. Eloul, C. Batchelor-McAuley, R.G. Compton, Thin film-modified electrodes: a model for the charge transfer resistance in electrochemical impedance spectroscopy, *J. Solid State Electrochem.* 18 (2014) 3239–3243. doi:10.1007/s10008-014-2662-1.
- [112] J. Kudr, L. Richtera, L. Nejd, K. Xhaxhiu, P. Vitek, B. Rutkay-Nedecky, D. Hynek, P. Kopel, V. Adam, R. Kizek, Improved electrochemical detection of zinc ions using electrode modified with electrochemically reduced graphene oxide, *Materials (Basel)*. 9 (2016) 1–12. doi:10.3390/ma9010031.
- [113] R.N. Vyas, B. Wang, Electrochemical analysis of conducting polymer thin films, *Int. J. Mol. Sci.* 11 (2010) 1956–1972. doi:10.3390/ijms11041956.
- [114] F. Electrode, Direct Electrochemical Detection of Bisphenol A Using a Highly Conductive Graphite Nanoparticle, (2017). doi:10.3390/s17040836.
- [115] R. Shen, W. Zhang, Y. Yuan, G. He, H. Chen, Electrochemical detection of bisphenol A at graphene/melamine nanoparticle-modified glassy carbon electrode, *J. Appl. Electrochem.* 45 (2015) 343–352. doi:10.1007/s10800-015-0792-5.